Enhanced Impedance-based Oscillatory Stability Assessment in Converter-dominated Power Systems

D. Hendriksma, C. Castrillón Franco, J. L. Rueda Torres*
Intelligent Electrical Power Grids, Delft University of Technology, Netherlands
*Corresponding author: j.l.ruedatorres@tudelft.nl

***Abstract*—The deployment of converter-dominated power systems introduces new oscillatory phenomena, which are difficult to accurately predict with existing assessment methods. This paper therefore proposes to enhance the classical impedance-based stability method with the objective of assisting in the quantitative assessment of subsynchronous oscillatory phenomena. To this end, vector fitting is applied to derive continuous state-space equations from measured impedance data and to subsequently deduce three stability indicators: sensitivity peak, oscillatory mode frequency and damping ratio. The proposed method was tested in an offshore wind-powered system and corroborated with time domain simulations for different shares of grid-following and grid-forming control. The results demonstrated that the indicators could capture the proximity to instability and the damping performance of critical converter-induced modes, hence enabling comparative investigations of parametric sensitivities.**

***Index Terms*—Offshore Power Systems, Impedance Scanning, Oscillatory Stability, Parametric Sensitivity Analysis.**

I. Introduction

In the forthcoming decades, an increasing share of energy is projected to be generated by renewable energy sources in order to fulfil the societal wish to reduce greenhouse gas emissions. However, the recent emergence of oscillatory phenomena in multi-converter power systems, such as offshore wind-powered networks, could give rise to subsynchronous oscillations (SSOs) induced by power electronic converters (PECs) that might compromise the operation and safety of those systems [1]–[4]. In comparison to synchronous generators (SGs), PECs inherently lack inertia and damping capability. Besides, the underlying mechanisms behind converter-induced SSOs are not well understood, but it is suspected that complex small-signal dynamics exerted by PEC controllers in subsynchronous range (such as phase-locked loops (PLLs) and current control) play an important role.

Analytical stability assessment methods, such as eigenvalue-based methods, may be inadequate for assessing the stability of converter-dominated power systems [1], [2]. Moreover, the nonlinear time-varying nature of PECs complicates the development of analytical models, where the intellectual property aspect poses further difficulties. On the contrary, measurement-based techniques, such as the impedance-based stability method, allow the system to be modelled as a black box, thereby bypassing the need for analytical models.

The aim of this paper is to propose an enhancement to the impedance-based stability method in order to advance the quantification and assessment of SSOs in converter-dominated systems. In addition, it allows identification of parametric sensitivities in the network. The paper is structured as follows: Section II covers the essentials of the classical impedance method and the proposed enhancement. In Section III, a description of a multi-converter offshore model is provided. Section IV then employs this model to demonstrate the proposed method by means of examining different control configurations. Finally, Section V comprises the conclusion.

II. Proposed Impedance-based Stability Method

A. Principle of Impedance Stability

The impedance-based stability method, first introduced in [5], is a frequency domain small-signal technique. It entails the division of grid-connected converter systems at the boundary of the interactions into a source and load subsystem [2], [6]. They are represented by a Thévenin and Norton circuit, each with an equivalent impedance Z_S and Z_L, respectively (Fig. 1). Firstly, the current through the point of common coupling (PCC) is determined:

$$\begin{aligned} I_{PCC}(s) &= \frac{Z_L(s)I_L(s) - V_S(s)}{Z_L(s) + Z_S(s)} \\ &= \left(I_L(s) - \frac{V_S(s)}{Z_L(s)}\right) \cdot \Big(1 + Z_S(s)/Z_L(s)\Big)^{-1} \end{aligned} \tag{1}$$

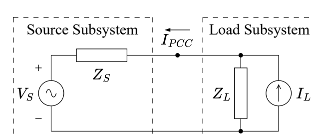

Fig. 1. Equivalent circuit for impedance stability analysis.

Given that the voltage source V_S is stable when unloaded and that the load Z_L is stable when powered from an ideal current source, the stability of the interconnected system is only dependant on the second term of (1). As the impedance method entails measurement of 3-phase impedances (e.g. dq-frame or sequence domain), a multi-input multi-output (MIMO) representation is used. Closed-loop matrix $\boldsymbol{T}(s)$, based on the impedance ratio $\boldsymbol{L}(s)$, can hence be derived:

$$\boldsymbol{T}(s) = \left[\boldsymbol{I}_n + \boldsymbol{L}(s)\right]^{-1} = \left[\boldsymbol{I}_n + \boldsymbol{Z}_S(s)\boldsymbol{Z}_L^{-1}(s)\right]^{-1} \tag{2}$$

The research shown in this paper has received funding from TenneT TSO B.V. within the FORBES research project: Adaptive Identification and Mitigation of Variable Oscillatory Phenomena in Weakening Networks. This work only reflects the authors' views, and the aforesaid organisation is not responsible for any use that may be made of the paper's content.

979-8-3315-8138-1

where $\boldsymbol{I}_n$ is the $n \times n$ identity matrix. Finally, the stability of the interconnected system can be evaluated with the generalised Nyquist stability criterion (GNSC) for MIMO systems by means of the frequency-dependant eigenloci $\lambda(s) = \{\lambda_1(s), \cdots, \lambda_n(s)\}$, which are computed with the characteristic polynomial $\Delta(\lambda(s))$ of $\boldsymbol{L}(s)$ [7]:

$$\det(\lambda(s) \cdot \boldsymbol{I}_n - \boldsymbol{L}(s)) \triangleq \Delta(\lambda(s)) \tag{3}$$

B. Impedance Frequency Scanning

The premise of the impedance method is that the equivalent impedances $\boldsymbol{Z}_S$ and $\boldsymbol{Z}_L$ can be measured for various operating conditions (i.e. obtaining snapshots for different network parametrisations or controller tuning). This approach facilitates comparative analyses and the detection of parametric sensitivities in power systems. In this work, measurements are conducted through AC impedance scans in a real-time digital simulator (RTDS) (Stage 1 in Fig. 2).

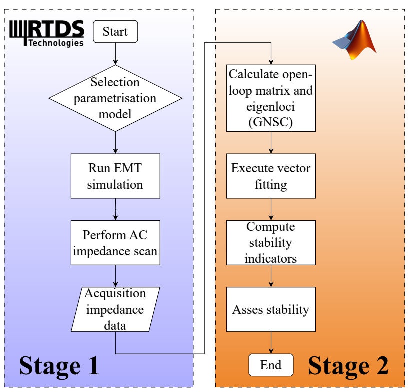

Fig. 2. Flowchart of implementation enhanced impedance method.

First, an electromagnetic transient (EMT) simulation is run on the simulator with the desired parametrisation. Since the impedance method is a small-signal method, it is important that the system operates in a steady-state condition prior to starting the impedance scan. If this prerequisite is met, voltage perturbations are injected along the SSO frequency range at the bipartition point of the power system. Thereafter, 3-phase small-signal responses are recorded in time domain and converted to dq-frame quantities. Discrete Fourier transform (DFT) is applied to obtain the impedance responses $\boldsymbol{Z}_S[f]$ and $\boldsymbol{Z}_L[f]$ per discrete frequency point.

C. Vector Fitting Operations

The stability of the system can be evaluated with the GNSC using the eigenloci $\lambda_{1,2}[f] = \text{eig}(\boldsymbol{L}[f])$. As $\boldsymbol{L}[f]$ and $\lambda_{1,2}[f]$ are discrete, a vector fitting algorithm, developed for MATLAB [8]–[10], is applied to obtain continuous transfer functions $\boldsymbol{L}(s)$ and $\lambda_{1,2}(s)$ from the impedance (Stage 2 in Fig. 2). This is done to facilitate stability quantification using a smooth, continuous response before applying the GNSC. Additionally, implementing the vector fitting algorithm improves the accuracy and robustness of the impedance data, as it can negate some of the measurement noise and mitigate the trade-off between scanning duration and step size by interpolating intermediate values in the data.

This algorithm iteratively solves a least squares problem for a given pole count. However, the number of poles of the measured impedance is not known a priori, which might lead to estimation errors and false poles. This could unintentionally result in incorrect stability conclusions, especially when fitting multi-terminal systems due to compounding errors [1]. To ensure accuracy, it is important that all resonances are captured and that the normalised root mean square error (NRMSE) reaches a magnitude below 10^{-1}.

D. Stability Quantification

This work proposes three stability indicators to improve the assessment of the oscillatory performance. They are derived from the vector-fitted state-space equations.

1) Sensitivity Peak: The sensitivity peak $1/\eta$ is a compact indicator that quantifies the proximity to instability [11], [12]. As showcased in Fig. 3, η is defined as the minimum distance between the Nyquist curve and the critical point $(-1, j0)$:

$$\eta = \min|1 + L(j\omega)| \;\Rightarrow\; 1/\eta = \max\left|\frac{1}{1 + L(j\omega)}\right| \tag{4}$$

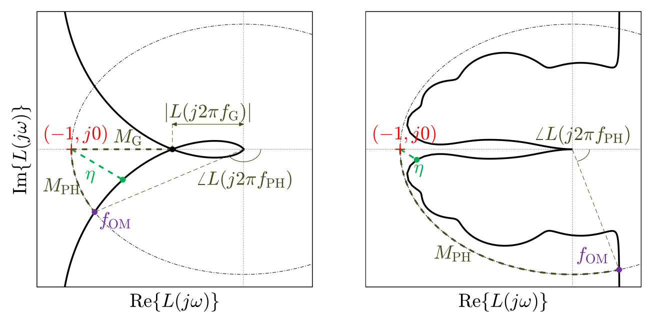

Fig. 3. Stability indicators visualised in Nyquist plot for arbitrary transfer function $L(j\omega)$. Left: lower order system. Right: higher order system with complex resonances.

High values for the sensitivity peak indicate that the system operates close to instability. Unlike the traditionally utilised gain margin M_{G} and phase margin M_{PH}, the sensitivity peak always provides the lowest available stability limit, thereby also considering the influence of complex resonances.

2) Oscillatory Mode Frequency: The frequency f_{OM} of the oscillatory mode (OM) can be determined at the frequency where the eigenloci intersect the unit circle in the Nyquist plot [1], [13] (Fig. 3). It is important to remark that only intersections close to the critical point are meaningful, as these intersections resemble true oscillatory frequencies. This can be explained by considering conjugate pole pair λ_{cp} located at the critical point:

$$\lambda_{cp} = \sigma_{cp} \pm j\omega_{cp} \quad \text{where: } L(\lambda_{cp}) = (-1, j0) \tag{5}$$

If the real part is small in comparison to the imaginary part, the Nyquist plot is essentially only dependant on the imaginary (oscillatory) part:

$$|\sigma_{cp}| \ll |\omega_{cp}| \;\Rightarrow\; L(j\omega_{cp}) \approx L(\sigma_{cp} \pm j\omega_{cp}) = (-1, j0) \tag{6}$$

979-8-3315-8138-1

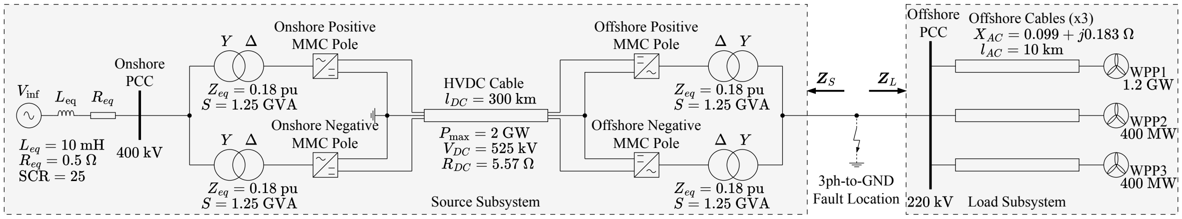

Fig. 4. Offshore test system.

This means that, when (6) is not satisfied, associated poles cannot be found in the Nyquist plot, resulting in neglection of non-critical oscillations [1]. It is thereby important to note that between the two eigenloci, the oscillatory frequency and sensitivity can only be inferred from the dominant eigenlocus because this locus is more likely to encircle $(-1, j0)$ [13].

3) Damping Ratio: The third indicator is the damping ratio ζ, which eases a comparison between the damping performance of different OMs [14]. The damping ratio can be obtained from the poles and zeros of the fitted state-space models; it is not immediately available from the discrete data. If one considers an arbitrary pole in the form $\lambda_k = \sigma_k + j\omega_k$, then ζ_k is defined as the real (damping) component normalised to the absolute value of the mode:

$$\zeta_k = \frac{-\sigma_k}{|\lambda_k|} \tag{7}$$

For most power networks, $\zeta_k \geq 5\%$ is deemed sufficient, as oscillations will dissipate within several seconds [15].

III. Offshore Test System

The impedance-based oscillatory stability analysis is conducted in the offshore test system depicted in Fig. 4. The topology of this system is adapted from an existing RTDS model [16], [17]. The subsystem impedances $\boldsymbol{Z}_S$ and $\boldsymbol{Z}_L$ are obtained by performing impedance scans at the offshore PCC, where the source-side comprises the equivalent onshore impedance Z_{eq}, a bipolar HVDC line with MMC poles. Meanwhile, the load side comprises three wind power plants (WPPs), with a combined capacity of 2 GW. Each WPP comprises an aggregated wind turbine (WT) model, where a scaling transformer multiplies the base power to the requisite rating of the WPP. The point of bipartition of the subsystems is selected at the offshore PCC in order to informatively analyse offshore-induced interactions. Furthermore, a 3-phase-to-ground fault disturbance is employed to trigger potential OMs of the system and to validate the impedance results with time domains simulations.

The offshore test system is modified by integrating grid-following (GFL) and grid-forming (GFM) control strategies in the WT converters, where the machine-side is represented as an ideal DC source. Fig. 5 displays the GFL-WT model, which incorporates a PLL that syncs the converter with the grid [3]. The PLL extracts the grid angle θ_g to enable the transformation from 3-phase domain (abc-domain) to the synchronous reference frame (dq-frame). Both the PLL and inner current loop are known to increase the converter output impedance [3], [18].

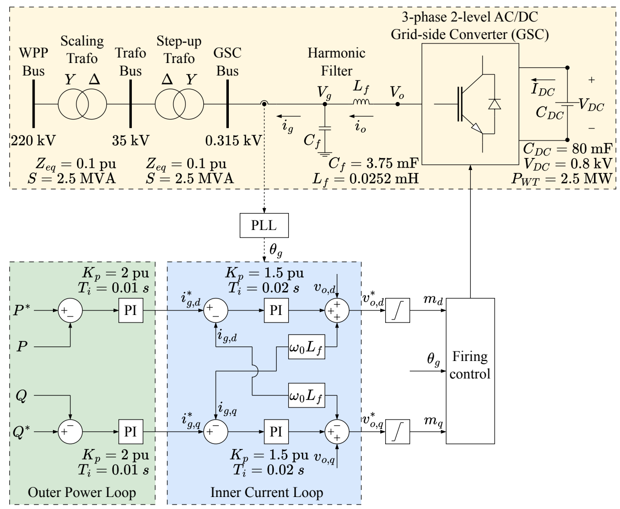

Fig. 5. Wind turbine model with GFL control.

Conversely, the GFM-WT converter adopts a virtual synchronous generator (VSG), which generates the phase angle θ locally (Fig. 6). It is equipped with inertia J and damping D_P, based on the swing equation of a SG, emulating the power synchronisation loop (PSL). The voltage and reactive power are controlled in the reactive control loop (QCL) [3]. Cascaded voltage and current loops are omitted, as the latter raises the output impedance of the converter [18].

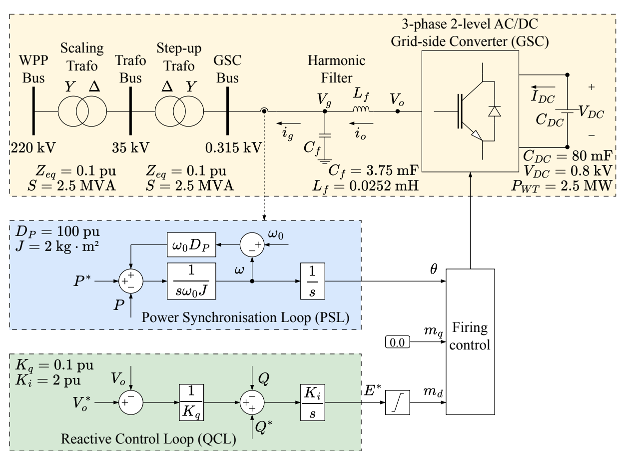

Fig. 6. Wind turbine model with GFM control.

979-8-3315-8138-1

IV. Case Study of WT Control Configurations

The aim of the case study is to test the proposed impedance methodology. To this end, the oscillatory susceptibility of the offshore test system is assessed by studying the impact of the WT controller configuration.

A. Case 1: 100% GFL

Case 1 studies the stability of the test system in the GFL-WT configuration by means of Nyquist and pole-zero plots (Fig. 7). The Nyquist graph showcases an OM at 44.49 Hz and illustrates that the system is operating close to instability, as the distance between the dominant locus and the critical point is small. Moreover, the right graph exposes the pole-zero locations and highlights that the critical OM has a damping ratio of only 3%.

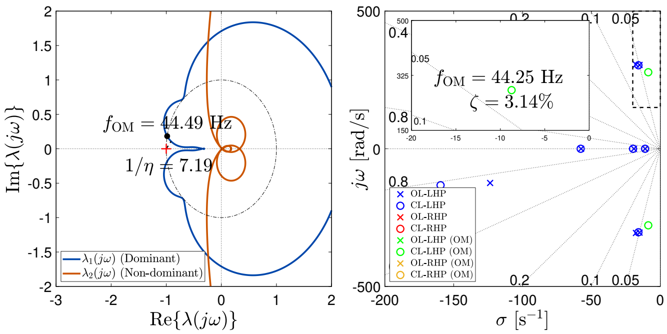

Fig. 7. Case 1: 100% GFL. Left: Nyquist plot. Right: pole-zero plot.

The impedance results are further exemplified by considering the time domain response of a 3-phase fault in Fig. 8. It can be observed that the power decays rapidly due to the absence of inertia. Furthermore, as no damping is present either, an unstable oscillation of 45.6 Hz appears. Ultimately, the system cannot recover from this fault and collapses, as it is no longer able to deliver 2 GW of power. Comparing the time domain results with the Nyquist analysis (Figs. 7 and 8), the impedance method predicts that the system is marginally stable, but in reality, it is unstable. The forecasted mode at 44.49 Hz appears as an unstable 45.6 Hz oscillation in time domain.

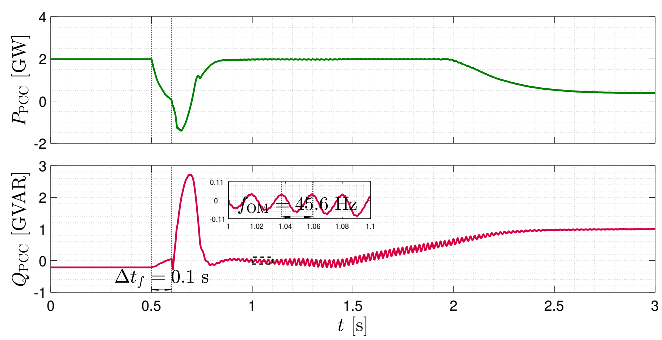

Fig. 8. Case 1: 100% GFL. 3-phase-to-ground fault during Δt_f. Top: active power P_{PCC}. Bottom: reactive power Q_{PCC}.

B. Case 2: 100% GFM

The second case utilises the same analysis to assess the performance of the GFM-WT configuration. Fig. 9 reveals that the oscillatory stability has improved, as the sensitivity has lowered significantly (from 7.19 to 2.16), while the damping of the detected OMs at 35.44 Hz and 67.86 Hz has improved from roughly 3% to 6%.

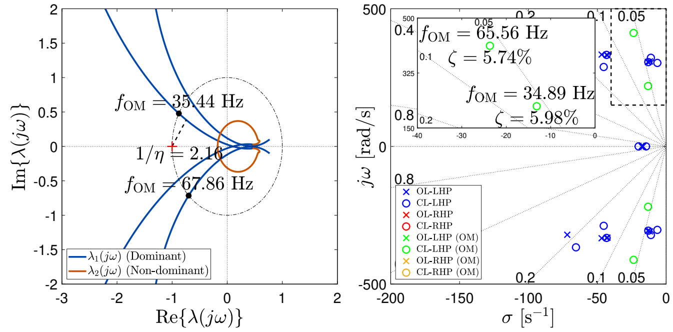

Fig. 9. Case 2: 100% GFM. Left: Nyquist plot. Right: pole-zero plot.

The time domain response in Fig. 10 exhibits that the power decay is limited by the active and reactive loops. The available damping capability ensures that system can restore its pre-fault operation after the initial transient. Besides, a well-damped 34.7 Hz oscillation is identified, which correlates with the mode found in the Nyquist and pole-zero plots.

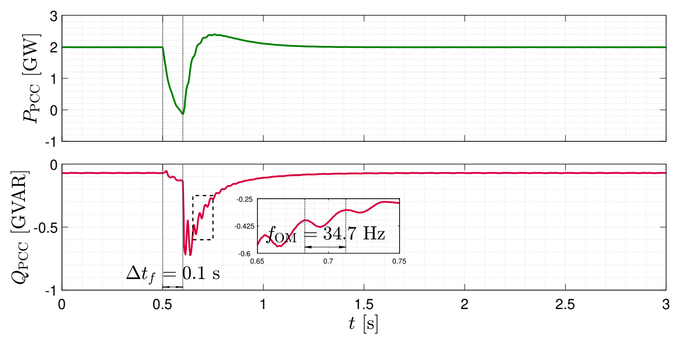

Fig. 10. Case 2: 100% GFM. 3-phase-to-ground fault during Δt_f. Top: active power P_{PCC}. Bottom: reactive power Q_{PCC}.

C. Case 3: Deployment Ratio GFL/GFM

Lastly, the oscillatory performance of the system is examined for different GFL/GFM deployment ratios. It is generally anticipated that the inertial response and the damping capacity of GFM improve the stability of converter-based networks. Nevertheless, GFL is suitable for strong systems, whilst GFM performs better in weak systems [19].

Three disadvantages to high shares of GFM are noteworthy. Firstly, synchronisation issues can occur when GFM converters are connected electrically close due to poor performance of the PSL when the impedance between converters is low [19]. Secondly, GFM controllers may simultaneously control the PCC voltage in parallel-coupled converter systems, which can result in adverse interactions, especially if the controllers are calibrated differently [20]. Lastly, fully emulating all WT converters as SGs has the downside that some of the inherent fast response and high controllability of PECs is lost [21].

The impact of GFM control is investigated in the offshore test system by increasing the GFM volume in steps of 20%, as listed in Table I. Among the ratios, it can be discerned that lower shares of GFM enhance the oscillatory performance in relation to 100% GFM. The indicators for 20–40% GFM show a lowered sensitivity peak and increased damping of $\sim$10%. This finding confirms that the optimal penetration of GFM is network-specific, determined by the inherent strength of the system, and thus an important design property.

TABLE I
CASE 3: STABILITY INDICATORS FOR DEPLOYMENT RATIOS GFL/GFM

Deployment ratio GFL/GFM	Sensitivity peak [-]	Mode frequency [Hz]	Damping ratio [%]
100% GFL / 0% GFM	7.19	44.25	3.14
80% GFL / 20% GFM	1.95	41.04 59.48	8.73 10.13
60% GFL / 40% GFM	1.84	38.13 66.23	9.94 12.63
40% GFL / 60% GFM	1.86	36.84 60.25	7.12 8.34
20% GFL / 80% GFM	1.86	36.49 64.06	6.52 6.99
0% GFL / 100% GFM	2.16	34.89 65.56	5.98 5.74

V. CONCLUSION

With the increasing share of renewable energy, it is expected that PEC-induced oscillations will occur more frequently in power systems. The complexity of analytical converter models and the intellectual property aspect necessitate a re-evaluation of existing stability assessment methodologies. This paper presented an enhancement of the impedance-based stability method. It consists of deducing three stability indicators (sensitivity peak, oscillatory frequency and damping ratio) derived from vector-fitted state-space models, which, in turn, are acquired by impedance measurements. The intend of the enhancement is twofold: firstly, to advance the quantitative assessment of converter-induced SSOs, and secondly, to foster insightful analyses of parametric sensitivities.

The proposed method was tested in an offshore wind-powered system and verified with time domain simulations. It was shown that the stability limits could be accurately estimated and that parametric differences related to varying shares of GFL/GFM could be comparatively assessed. The results illustrated that GFL leaves the system highly susceptible to a subsynchronous OM. In comparison, GFM and notably lower shares of GFM yield lowered sensitivity and improved damping performance.

REFERENCES

[1] Q. Chen, S. Bu, and C. Y. Chung, "Small-Signal Stability Criteria in Power Electronics-Dominated Power Systems: A Comparative Review," *J. Mod. Power Syst. Clean Energy*, vol. 12, no. 4, pp. 1003–1018, Jul. 2024.

[2] M. Val Escudero, G. Lietz, Y. Liao, Q. Zhang, and J. Lu, "Linear Analysis Methods to Characterize Inherent Small-Signal Behavior of the Plant and Overall Power System," in *Power System Dynamic Modelling and Analysis in Evolving Networks*, ser. CIGRE Green Books, B. Badrzadeh and Z. Emin, Eds. Springer Nature Switzerland AG, 2024, pp. 263–307.

[3] H. Zhang, W. Xiang, W. Lin, and J. Wen, "Grid Forming Converters in Renewable Energy Sources Dominated Power Grid: Control Strategy, Stability, Application, and Challenges," *J. Mod. Power Syst. Clean Energy*, vol. 9, no. 6, pp. 1239–1256, Nov. 2021.

[4] V. Sewdien, X. Wang, J. Rueda Torres, and M. van der Meijden, "Critical Review of Mitigation Solutions for SSO in Modern Transmission Grids," *Energies*, vol. 13, no. 13, p. 3449, Jul. 2020.

[5] R. D. Middlebrook, "Input filter consideration in design and application of switching regulators," in *IEEE Ind. Appl. Soc. Annu. Meet.*, Nov. 1976, pp. 366–382.

[6] J. Sun, "Impedance-Based Stability Criterion for Grid-Connected Inverters," *IEEE Trans. Power Electron.*, vol. 26, no. 11, pp. 3075–3078, Nov. 2011.

[7] B. Wen, R. Burgos, D. Boroyevich, P. Mattavelli, and Z. Shen, "AC Stability Analysis and dq Frame Impedance Specifications in Power-Electronics-Based Distributed Power Systems," *IEEE J. Emerg. Sel. Top. Power Electron.*, vol. 5, no. 4, pp. 1455–1465, Dec. 2017.

[8] B. Gustavsen and A. Semlyen, "Rational approximation of frequency domain responses by vector fitting," *IEEE Trans. Power Deliv.*, vol. 14, no. 3, pp. 1052–1061, Jul. 1999.

[9] B. Gustavsen, "Improving the pole relocating properties of vector fitting," *IEEE Trans. Power Deliv.*, vol. 21, no. 3, pp. 1587–1592, Jul. 2006.

[10] D. Deschrijver, M. Mrozowski, T. Dhaene, and D. De Zutter, "Macromodeling of Multiport Systems Using a Fast Implementation of the Vector Fitting Method," *IEEE Microw. Wirel. Compon. Lett.*, vol. 18, no. 6, pp. 383–385, Jun. 2008.

[11] A. G. Yepes, F. D. Freijedo, Ó. Lopez, and J. Doval-Gandoy, "Analysis and Design of Resonant Current Controllers for Voltage-Source Converters by Means of Nyquist Diagrams and Sensitivity Function," *IEEE Trans. Ind. Electron.*, vol. 58, no. 11, pp. 5231–5250, Nov. 2011.

[12] I. D. Landau, "The R-S-T digital controller design and applications," *Control Eng. Pract.*, vol. 6, no. 2, pp. 155–165, Feb. 1998.

[13] Y. Liao, Z. Liu, H. Zhang, and B. Wen, "Low-Frequency Stability Analysis of Single-Phase System With dq-Frame Impedance Approach—Part II: Stability and Frequency Analysis," *IEEE Trans. Ind. Appl.*, vol. 54, no. 5, pp. 5012–5024, Sep. 2018.

[14] P. Kundur, *Power System Stability and Control*. McGraw-Hill, 1994.

[15] F. R. S. Sevilla and L. Vanfretti, "A small-signal stability index for power system dynamic impact assessment using time-domain simulations," in *2014 IEEE PES Gen. Meet. Conf. Expo.*, Jul. 2014, pp. 1–5.

[16] A. Shetgaonkar, M. Popov, A. Lekić, and T. Karmokar, "Enhanced Real-Time Multi-Terminal HVDC Power System Benchmark Models with Performance Evaluation Strategies," *CIGRE Sci. Eng.*, vol. 32, pp. 1–29, Feb. 2024.

[17] L. Liu, A. Shetgaonkar, and A. Lekić, "Interoperability of classical and advanced controllers in MMC based MTDC power system," *Int. J. Electr. Power Energy Syst.*, vol. 148, p. 108980, Jun. 2023.

[18] C. Henderson, A. Egea-Alvarez, P. Papadopoulos, R. Li, L. Xu, R. Da Silva, A. Kinsella, I. Gutierrez, and R. Pabat-Stroe, "Exploring an Impedance-Based SCR for Accurate Representation of Grid-Forming Converters," in *2022 IEEE Power Energy Soc. Gen. Meet. PESGM*, Jul. 2022, pp. 1–5.

[19] R. Rosso, X. Wang, M. Liserre, X. Lu, and S. Engelken, "Grid-Forming Converters: Control Approaches, Grid-Synchronization, and Future Trends—A Review," *IEEE Open J. Ind. Appl.*, vol. 2, pp. 93–109, Apr. 2021.

[20] C. Henderson, A. Egea-Alvarez, and L. Xu, "Analysis of optimal grid-forming converter penetration in AC connected offshore wind farms," *Int. J. Electr. Power Energy Syst.*, vol. 157, p. 109851, Jun. 2024.

[21] Q. Peng, Q. Jiang, Y. Yang, T. Liu, H. Wang, and F. Blaabjerg, "On the Stability of Power Electronics-Dominated Systems: Challenges and Potential Solutions," *IEEE Trans. Ind. Appl.*, vol. 55, no. 6, pp. 7657–7670, Nov. 2019.

979-8-3315-8138-1